Water Research 261 (2024) 121965

Contents lists available at ScienceDirect

Water Research

journal homepage: www.elsevier.com/locate/watres

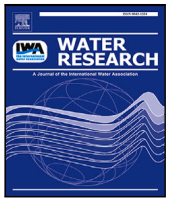

Mercury cycling in contaminated coastal environments: modeling the benthic-pelagic coupling and microbial resistance in the Venice Lagoon

Ginevra Rosati [a,*], Cosimo Solidoro [a,c], Célia Laurent [a], Leslie Aveytua Alcázar [a], Georg Umgiesser [b], Donata Canu [a]

[a] National Institute of Oceanography and Applied Geophysics - OGS, Trieste, 34010, Italy
[b] Istituto di Scienze Marine, ISMAR-CNR, Venice, 30125, Italy
[c] International Centre for Theoretical Physic, ICTP, Trieste, 34010, Italy

ARTICLE INFO

Dataset link: DOI:10.5281/zenodo.11933313, https://zenodo.org/records/11933313

Keywords:
Mercury
Methylmercury
Pollution
Model
Coastal
SHYFEM

ABSTRACT

Anthropogenic activities have been releasing mercury for centuries, and despite global efforts to control emissions, concentrations in environmental media remain high. Coastal sediments can be a long-term repository for mercury, but also a secondary source, and competing processes in marine ecosystems can lead to the conversion of mercury into the toxic and bioaccumulative species methylmercury, which threatens ecosystem and human health. We investigate the fate and transport of three mercury species in a coastal lagoon affected by historical pollution using a novel high-resolution finite element model that integrates mercury biogeochemistry, sediment dynamics and hydrodynamics. The model resolves mercury dynamics in the seawater and the seabed taking into account partitioning, transport driven by water and sediment, and photochemical and microbial transformations. We simulated three years (early 2000s, 2019, and 2020) to assess the spatio-temporal distribution of mercury species concentrations and performed a sensitivity analysis to account for uncertainties. The modeled mercury species concentrations show high temporal and spatial variability, with water concentrations in some areas of the lagoon exceeding those of the open Mediterranean Sea by two orders of magnitude, consistent with available observations from the early 2000s. The results support conclusions about the importance of different processes in shaping the environmental gradients of mercury species. Due to the past accumulation of mercury in the lagoon sediments, inorganic mercury in the water is closely related to the resuspension of contaminated sediments, which is significantly reduced by the presence of benthic vegetation. The gradients of methylmercury depend on the combination of several factors, of which sediment resuspension and mercury methylation are the most relevant. The results add insights into mercury dynamics at coastal sites characterized by a combination of past pollution (i.e. sediment enrichment) and erosive processes, and suggest possible nature-based mitigation strategies such as the preservation of the integrity of benthic vegetation and morphology.

1. Introduction

Mercury (Hg) is a persistent pollutant detrimental to ecosystems and human health (Chen et al., 2016), due to the bioaccumulation of its organic species methylmercury (MeHg) (Philibert et al., 2022), a neurotoxic compound microbially produced in seawater and sediments from inorganic oxidized mercury (Hg^{II}) (see Bowman et al. (2020) and Cossa et al. (2022) and references therein). Coastal sediments are often enriched in Hg of anthropogenic origin (Acquavita et al., 2012; Conaway et al., 2003; Schartup et al., 2013; Sprovieri et al., 2011; Zonta et al., 2018), and often act as a secondary source of legacy Hg and MeHg to the water column over the long-term (Bloom et al., 2004; Canu and Rosati, 2017; Rosati et al., 2020; Seelen et al., 2021), even after remedial dredging (Matsuyama et al., 2021; Soetan et al., 2022). Management of sites historically contaminated by industrial sources is challenging, but critical to protect local communities from Hg exposure (Hsu-Kim et al., 2018; Bravo et al., 2010; Gibičar et al., 2009).

Environmental Hg and MeHg concentrations are controlled by several physical and biogeochemical factors that can be highly heterogeneous in time and space, and fate and transport models contribute to the assessment of Hg dynamics by simulating key processes and the interactions that influence their complex evolution. Indeed, previous studies have shown that MeHg in sediment is not simply correlated with total Hg concentration (Hg_T) (Acquavita et al., 2012; Hollweg et al., 2009; Sunderland et al., 2006; Schartup et al., 2013; Zhang et al., 2014), and that sediment concentrations of Hg or MeHg are

* Corresponding author.
E-mail address: grosati@ogs.it (G. Rosati).

https://doi.org/10.1016/j.watres.2024.121965
Received 26 June 2023; Received in revised form 17 June 2024; Accepted 18 June 2024
Available online 22 June 2024

poor predictors of concentrations in water (Balcom et al., 2015; Seelen et al., 2021; Conaway et al., 2003) and biota (Chen et al., 2014; Mason et al., 2023). The correlation between Hg concentrations in sediments and water becomes significant only at anthropogenically impacted sites where internal recycling dominates over external inputs (Seelen et al., 2021), and tight benthic-pelagic coupling is also favored by shallow waters, high sediment resuspension, and abundance of organic carbon (Bloom et al., 2004; Melaku Canu et al., 2015; Conaway et al., 2003; Rosati et al., 2020; Seelen et al., 2018). The importance of the benthic-pelagic coupling decreases seaward so that sediment resuspension is generally neglected in oceanic models for Hg (e.g. Rosati et al. (2022), Zhang et al. (2015, 2020) and Soerensen et al. (2016)), and specific tools need to be developed to inform the management of coastal ecosystems. Other peculiarities of contaminated coastal sites include differences in the relative importance of river input, bioavailability of Hg species, and local adaptations of the microbial communities. Rivers affect coastal dynamics of Hg through direct input of Hg species (Liu et al., 2021) and by supplying organic matter that can fuel the microbial community enhancing Hg methylation (Liu et al., 2023) but at the same time can reduce Hg bioavailability limiting bacteria and phytoplankton uptake and bioaccumulation (Schartup et al., 2015; Seelen et al., 2023). However, terrestrial organic matter affects also the bioavailability of MeHg, possibly reducing its degradation and causing high MeHg concentrations at sites where the methylation rates are low (Bravo et al., 2017). The bioavailability of Hg species is also modulated by lithogenic material and hydroxides of iron and manganese that act as scavengers of dissolved Hg species (Lamborg et al., 2016). Desorption of Hg from lithogenic material is negligible (Lamborg et al., 2016), while hydroxides can undergo dissolution and release the associated Hg in suboxic conditions (Emili et al., 2014).

High contamination exerts a selective pressure on microbial communities that favors coping strategies such as resistance to heavy metals (Banchi et al., 2023). Microbial resistance to Hg depends on a set of genes, clustered in the "mer operon", which mediate the elimination of inorganic Hg from the cell and also of MeHg in broad-spectrum resistance by converting it to gaseous Hg^0 (Barkay et al., 2003). Demethylation associated with the production of Hg^0 rather than Hg^{II} has been detected in sediments (Hines et al., 2012; Baldi et al., 2012; Marvin-DiPasquale et al., 2000) and surface water (Schaefer et al., 2004) from contaminated ecosystems, and in the latter study, mer genes were found in a wetland contaminated by a chloralkali site but not at other sites. The authors highlighted a negative correlation between the proportion of Hg_T as MeHg and Hg_T concentration, which could explain some of the variability observed in larger data sets. In the sediments of the Venice Lagoon, Hg resistance genes were found in higher abundance ($0.009 \pm 0.001\%$) near industrial pollution sources than in less impacted sampling stations ($0.004 \pm 0.002\%$) (Banchi et al., 2021). Mer genes and transcripts have also been detected in the oceanic water column, despite the relatively low Hg concentrations (Sanz-Sáez et al., 2022).

Historical Hg inputs from a chlor-alkali plant, active from 1950 to the early 2000s, have led to widespread contamination of the sediment of the Venice Lagoon (Mediterranean Sea), especially near industrial sources (MAV-CVN, 1999; Critto et al., 2005; Guédron et al., 2012; Han et al., 2007; Zonta et al., 2018). The available water data, which are more limited in time and space, also show high concentrations (up to 1 pM of MeHg and > 100 pM of Hg_T) (Guédron et al., 2012; Bloom et al., 2004). Hg concentrations in bivalves and low trophic level fish are 2–4 times higher than in the Mediterranean Sea (Dominik et al., 2014). The lagoon is a valuable ecosystem and UNESCO World Heritage Site. Artisanal and small-scale fisheries and aquaculture are important cultural and economic resources for the local community, and over the past decades, there has been continuous research to manage the multiple natural (Solidoro et al., 2004; Sfriso et al., 2001; Sfriso and Marcomini, 1996; Solidoro et al., 2010; Bandelj et al., 2008, 2009) and anthropogenic (Solidoro et al., 2010; Marcomini et al., 2000; Zonta et al., 2018; Cossarini et al., 2008) pressures challenging its fragile ecological and socio-economic equilibrium (Canu et al., 2011; Sfriso et al., 2020; Rapaglia et al., 2015; Solidoro et al., 2010). Ecological risk assessments indicate the need for strengthening Hg monitoring (Picone et al., 2023; Critto et al., 2005; Micheletti et al., 2004).

We coupled a module for Hg biogeochemistry, a novel module for sediment dynamics, and a hydrodynamic finite element model to estimate the spatial and temporal variability of Hg species concentration in the Venice Lagoon. The resulting integrated model is designed for contaminated coastal sites because it combines: (1) a hydrodynamic model (Umgiesser et al., 2004) that uses an unstructured finite element mesh that can approximate bathymetry and coastal geometry at very high resolution, (2) a Hg module that describes the fate of Hg^{II}, MeHg, and Hg^0 (Melaku Canu et al., 2015; Rosati et al., 2018, 2020; Wool et al., 2001), and is here extended to include a novel parametrization for microbial Hg resistance, and (3) a model for benthic-pelagic coupling of sediment and Hg species that also accounts for the sheltering effect of benthic vegetation on sediment resuspension (Marani et al., 2013; Carniello et al., 2014; Neto et al., 2022) and tracks the morphodynamic evolution of the seabed. All of these features are extremely relevant for modeling Hg in contaminated coastal sites. Indeed, coastal environments and lagoons often present rather complex bathymetries and morphological features that can hardly be captured by finite difference parametrization. The benthic-pelagic coupling, if taken into account, is usually represented through prescribed rates and not explicitly related to the bottom shear stress (Melaku Canu et al., 2015; Rosati et al., 2020; Bieser et al., 2023). Microbial Hg resistance has never been tested in a model, and a contaminated site such as the Venice Lagoon is ideal for testing its potential to affect environmental concentrations. The model was used to characterize Hg dynamics in three years (early 2000s, 2019 and 2020) with different oceanographic and meteorological conditions. The relative importance of different processes in shaping the magnitude and gradients of Hg concentration in sediments and water of the lagoon and similar environments is estimated through sensitivity analysis.

2. Methods

A dynamic model (Fig. 1a) simulating: (i) Hg biogeochemistry (Melaku Canu et al., 2015; Rosati et al., 2020; Wool et al., 2001) (Section 2.1), (ii) sediment dynamics (Section 2.2), and (iii) hydrodynamic properties and transport (Section 2.3) was developed, calibrated, validated and used to investigate the fate and transport of three Hg species Hg_i (oxidized Hg - Hg^{II}, methylmercury - MeHg, and elemental Hg - Hg^0) in waters and sediments of the Venice Lagoon for three years (Section 2.4), also assessing model sensitivity (Section 2.4.2).

The integrated SHYFEM-Hg model (Supplementary Figure 1) is spatially discretized over an unstructured mesh (Fig. 1b) with variable element resolution, ranging from about 10 m in the more morphologically complex areas and the channel systems to 1 km over some homogeneous tidal flats. In each element, the model simulates the evolution of physical and biogeochemical state variables based on meteorological and hydrodynamic input data (Supplementary Figures 2 and 3) and prescribed boundary concentrations, running with a time step of 300 s. The sediment module simulates the dynamics of three different kinds of particles P_i (fine inorganic particles — silt, refractory organic matter, and labile organic matter) and accounts for sediment erosion and deposition and particle-mediated transport of Hg species. The hydrodynamical model handles the hydrodynamic transport of suspended sediment particles and Hg species and modulates the bottom shear stress triggering erosion and deposition. The partition, transformations, and degassing of Hg species are tracked by the mercury module. A detailed description of the model equations and usage is provided in Supplementary Material 1 (user manual). The code of the model is open source and available in the Zenodo repository with DOI 10.5281/zenodo.11933313.

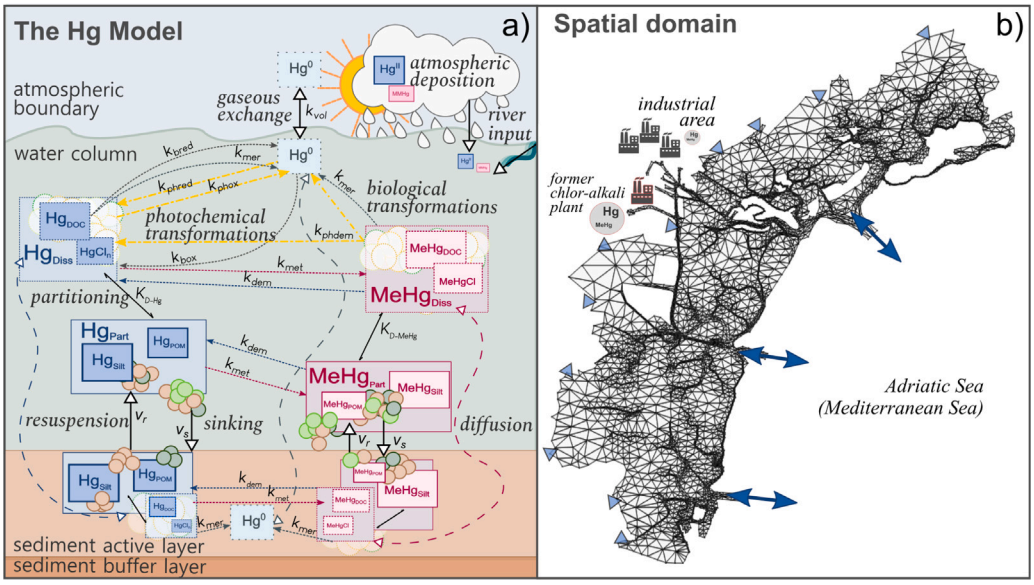

Fig. 1. (a) Overview of the Hg cycle processes simulated in the SHYFEM-Hg model and (b) grid of the finite element model for the Venice Lagoon showing the location of the inlets (bidirectional blue arrows), river discharge (light blue triangles), and the industrial area. The conceptual model (a) represents the fate of the three Hg species: inorganic oxidized Hg (Hg^{II}, blue squares), gaseous elemental Hg (Hg^0, cyan square), and methylmercury (MeHg, purple squares). All Hg species undergo photochemical (photoreduction, photooxidation, and photodemethylation) and biological (methylation and demethylation) transformations (dashed arrows) at rates k_x. Hg^0 is exchanged with the atmosphere as a function of wind speed and temperature (k_{tvol}). Hg^{II} and MeHg distribute among dissolved and particulate phases based on partition coefficients $K_{D_{Hg_i}-P_i}$ and are subjected to particle-mediated deposition to and resuspension from the seabed. Other transport processes include atmospheric deposition, input from rivers, and hydrodynamic exchanges. (For interpretation of the references to color in this figure legend, the reader is referred to the web version of this article.)

2.1. The mercury model

Following previous work (Melaku Canu et al., 2015; Wool et al., 2001), the mercury model (Supplementary material 1.2) simulates the main processes affecting the fate of three state variables Hg_i (μg m^{-3}) (Fig. 1a) according to Eqs. (1) (water) and (2) (sediment). In each water or sediment point (j) of the model, the three Hg species are linked by biogeochemical transformations (bgc) modeled as linear kinetics (Supplementary Table 5) and other Hg fluxes related to resuspension ($J^{res}_{Hgi_s}$) and deposition ($J^{dep}_{Hgi_w}$) of particles, and to pore-water diffusion ($J^{pwd}_{Hgi_{s-w}}$) (Supplementary Table 6). The Hg state variables in water are subject to advection, diffusion, and boundary exchange. Monthly-variable river loadings ($L^{riv}_{Hgi_w}$) enter the basin in correspondence with river mouths. Atmospheric deposition ($L^{atm}_{Hgi_w}$) is imposed as spatially homogeneous loads of Hg^{II} and MeHg. Based on partition coefficients ($K_{D_{Hgi}-P_i}$), Hg^{II} and MeHg are partitioned between dissolved phases ($Hg^{II}_{diss} = Hg^{II}_{DOC} + HgCl_n$, $MeHg_d = MeHg_{DOC} + MeHgCl$) and particulate phases associated to silt and particulate organic matter ($Hg^{II}_{part} = Hg^{II}_{POM} + Hg^{II}_{silt}$, and $MeHg_p = MeHg_{POM} + MeHg_{silt}$) (Supplementary Table 4). Hg^0, instead, is generally found as a dissolved gas in seawater and is neither associated ($K_{D_{Hg^0}-P_i} = 0$) nor transported by particles ($J^{dep}_{Hg^0_w} = 0$, $J^{res}_{Hg^0_s} = 0$). Hg^0 is the only species that is exchanged with gaseous atmospheric mercury ($J^{evs}_{Hg^0_w} \neq 0$).

$$\frac{\partial Hg_{i,w(x,y)}}{\partial t} = \underbrace{-u\frac{\partial Hg_{i,w}}{\partial x} - v\frac{\partial Hg_{i,w}}{\partial y}}_{\text{Advection}} + \underbrace{K_h\left(\frac{\partial^2 Hg_{i,w}}{\partial x^2} + \frac{\partial^2 Hg_{i,w}}{\partial y^2}\right)}_{\text{Turbulent Diffusion}} + \underbrace{J^{bgc}_{Hg_{i,w}}}_{\text{Transformations}} \underbrace{-J^{dep}_{Hg_{i,w}} + J^{res}_{Hg_{i,s}}}_{\text{Particle-mediated transport}} \underbrace{-J^{pwd}_{Hg_{i,s-w}}}_{\text{Porewater Diffusion}} \underbrace{-J^{evs}_{Hg_{i,w}}}_{\text{Evasion}} \underbrace{+L^{riv}_{Hg_{i,w}} + L^{atm}_{Hg_{i,w}}}_{\text{Loads}} \quad (1)$$

$$\frac{\partial Hg_{i,s(x,y)}}{\partial t} = \underbrace{J^{bgc}_{Hg_{i,s}}}_{\text{Transformations}} + \underbrace{J^{dep}_{Hg_{i,w}} - J^{res}_{Hg_{i,s}}}_{\text{Particle-mediated transport}} \underbrace{+J^{pwd}_{Hg_{i,s-w}}}_{\text{Porewater Diffusion}} \quad (2)$$

Transformations of Hg species (Supplementary Equation 47–57) are described as first-order kinetics corrected for temperature (biotic reactions) or light availability (photochemical reactions), in turn depending on irradiance, extinction coefficient, and water depth. Microbial resistance to Hg is introduced by adding mer-mediated reductive demethylation and Hg^{II} reduction in water and porewater with an activation threshold at 50 pM (10 ng l^{-1}) (Rasmussen and Turner, 1997).

Hg species in the seabed are initialized (Supplementary Table 8, Eqs. 78–80) from concentrations in μg g^{-1}, as usually available from field studies, and converted to volumetric concentrations (μg m^{-3}) of particulate (Hg^{II}_{part} and $MeHg_{part}$) and pore-water dissolved ($Hg^{II}_{d(s)}$ and $MeHg_{d(s)}$) concentrations, taking into account concentrations of sediment particles (P_i) and porosity (ϕ) (Thomann and Di Toro, 1983) provided by the sediment module. All model state variables can be initialized with spatially variable concentrations (e.g., Fig. 2a–b).

2.2. The sediment model

The sediment model (Supplementary Text 1.3) simulates three state variables P_i (g m^{-3}) in water (Eq. (3)) and sediment (Eq. (4)). The labile particulate organic matter (POM_{lab}) represents the plankton component, it is degraded at a fast pace (Stolpovsky et al., 2018) and produced in the water as a function of temperature, while POM_{ref}, represents refractory organic matter, has a longer turnover time ($J^{deg}_{POM_{ref}} \ll J^{deg}_{POM_{lab}}$) and enters the water through river input and sediment resuspension. River and resuspension/deposition dynamics also control the silt state variable, which represents the fine inorganic particles and thus

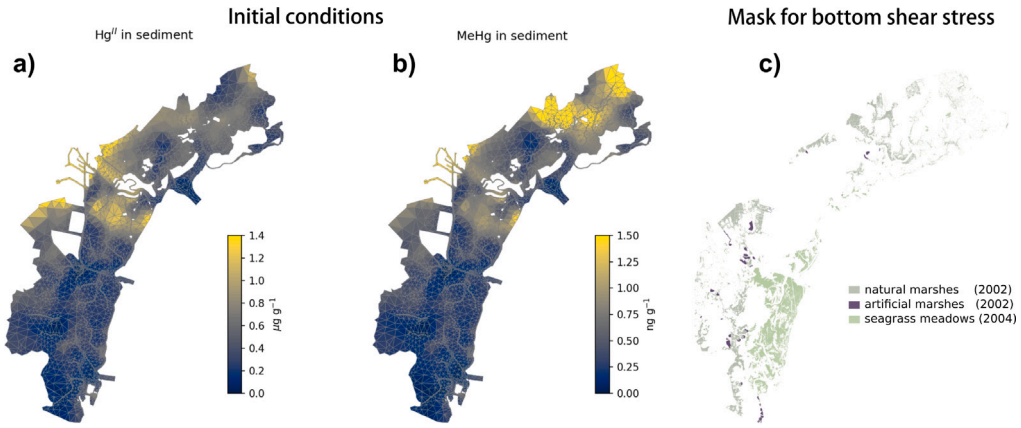

Fig. 2. Spatially variable initial condition for sediment concentrations of (a) Hg^{II} ($\mu g\,g^{-1}$) (Zonta et al., 2018; Bellucci et al., 2002) and (b) MeHg ($ng\,g^{-1}$) (Rosati et al., 2020) in the Venice Lagoon. Panel (c) shows the mask of salt marshes and seagrasses used to modulate sediment resuspension (see Sections 2.2 and 2.4).

has null rates of degradation and production ($J^{deg}_{silt} = 0$ and $J^{PP}_{silt} = 0$).

$$\frac{\partial P_{i,w(x,y)}}{\partial t} = \underbrace{-u\frac{\partial P_{i,w}}{\partial x} - v\frac{\partial P_{i,w}}{\partial y}}_{\text{Advection}} + \underbrace{K_h\left(\frac{\partial^2 P_{i,w}}{\partial x^2} + \frac{\partial^2 P_{i,w}}{\partial y^2}\right)}_{\text{Turbulent Diffusion}} + \underbrace{-J^{dep}_{P_{i,w}} + J^{res}_{P_{i,s}}}_{\text{Deposition/resuspension}} \underbrace{- J^{deg}_{P_{i,w}}}_{\text{Degradation}} \underbrace{+ J^{PP}_{P_{i,w}}}_{\text{Production}} \underbrace{+ L^{riv}_{P_{i,w}}}_{\text{Loads}} \quad (3)$$

$$\frac{\partial P_{i,s(x,y)}}{\partial t} = \underbrace{J^{dep}_{P_{i,w}} - J^{res}_{P_{i,s}}}_{\text{Deposition/Resuspension}} \underbrace{- J^{deg}_{P_{i,s}}}_{\text{Degradation}} \quad (4)$$

Silt and POMs are dynamically exchanged between the water column and the seabed ($J^{dep}_{P_{i,w}}, J^{res}_{P_{i,s}}$), depending on the sediment properties (Supplementary Table 9) and the bottom shear stress (τ_b, Pa) computed by the hydrodynamic module. Sediment erosion and deposition are parameterized following Supplementary Equations 83–92. Sediment properties (i.e., bulk and dry densities) are calculated using the equations for flooded sediments (Supplementary Equations 100–103) described in Avnimelech et al. (2001).

The model tracks the morphodynamic evolution of the seabed by updating the thickness of the sediment surface layer in response to the net fluxes of deposition/erosion. Below this active surface layer is a buffer subsurface layer with constant sediment concentrations (Carniello et al., 2012). As described by Exner's equation (Supplementary Table 9, Eq. 106), in case of net deposition the thickness of the active layer increases. When resuspension exceeds deposition, the surface layer is eroded until a critical sediment thickness (Z_0 = 2 cm). Below this threshold, the thickness erosion is compensated by incorporating sediment from the buffer layer.

The sheltering effect of landforms and benthic vegetation (Marani et al., 2013; Carniello et al., 2014; Neto et al., 2022) can be simulated by employing a mask (e.g., Fig. 2c) that reduces the bottom shear stress values to zero in the areas of concern, thus suppressing sediment resuspension and maximizing sediment settling (Supplementary Text 1.3 and 1.4).

2.3. The SHYFEM model

SHYFEM is an open-source hydrodynamic model that has already been used to study hydrodynamics (Umgiesser et al., 2004) and biogeochemical dynamics of the Venice Lagoon (Umgiesser et al., 2003; Melaku Canu et al., 2003) and other lagoons or coastal areas (Aveytua-Alcazar et al., 2020; Ferrarin et al., 2010; Melaku Canu et al., 2016; Umgiesser et al., 2014). The SHYFEM model solves the shallow water equations on a finite element grid, in their formulation with transports. The integration in time is performed using a semi-implicit algorithm that combines the advantages of the explicit and the implicit scheme. Modeled state variables include water temperature and salinity, water levels, and current speed and direction. In Eqs. (5)–(7), U and V are the vertical integrals in x and y directions of the horizontal velocities u and v (total or barotropic transport) (Eqs. (8)–(9)), $H = h+\zeta$ is the total water depth, and ζ the water level. R is the friction coefficient determined through the Strickler formula, f is the Coriolis parameter, g is the gravitational acceleration, and t is time. The terms X and Y contain all other terms that can be treated explicitly by the semi-implicit algorithm, such as the wind stress and the horizontal eddy viscosity, which is parameterized through the Smagorinsky scheme (Smagorinsky, 1963). The boundary conditions for stress terms (wind stress and bottom drag) follow a quadratic parametrization. Heat fluxes are computed at the water surface, and air–sea water fluxes depend on the balance between precipitation and evaporation.

$$\frac{\partial U}{\partial t} - fV + gH\frac{\partial \zeta}{\partial x} + RU + X = 0 \quad (5)$$

$$\frac{\partial V}{\partial t} + fU + gH\frac{\partial \zeta}{\partial y} + RV + Y = 0 \quad (6)$$

$$\frac{\partial \zeta}{\partial t} + \sum \frac{\partial U}{\partial x} + \frac{\partial V}{\partial y} = 0 \quad (7)$$

$$U = \int_{-h}^{\zeta} u\,dz \quad (8)$$

$$V = \int_{-h}^{\zeta} v\,dz \quad (9)$$

2.4. Setup for the Venice Lagoon

We simulated the Hg dynamics in the Venice Lagoon for the early 2000s to calibrate the model against the observed concentrations of suspended particulate matter (SPM) and particulate organic matter (POM) in the lagoon and validate it against available observations of Hg species (Bloom et al., 2004). We then used the calibrated model to simulate present-day dynamics (2019 and 2020) and assess model sensitivity (Section 2.4.2).

The simulations rely on realistic meteorological forcings (irradiance, wind speed, air temperature, and humidity) and hydrodynamic data (water levels, temperature, and salinity at the inlets, river discharge, and temperature) for each year (MAV-CVN, 2005; ISPRA Ambiente, 2023) (Supplementary Figures 2 and 3), with hydrodynamic fluxes including the contribution from eleven tributaries and bidirectional exchanges at the lagoon inlets (Fig. 1b). The initial conditions (i.e., concentrations of Hg and particles in the seabed) and boundary conditions (i.e., Hg concentrations in the river, seawater, and atmosphere) are

instead fixed in the three simulations and the impacts of their variations are explored through sensitivity analysis. Such an approach makes it possible to distinguish between the effects of inter-annual meteorological variability and changes in Hg concentrations.

The Hg loadings from the rivers and the sea are calculated by the model based on time-variable realistic hydrodynamic fluxes and fixed boundary concentrations of the three Hg species (Supplementary Table 13) (Bloom et al., 2004; Rossini et al., 2005; Kotnik et al., 2015).

Initial conditions for Hg^{II} in sediment (Fig. 2a) are obtained from field data of Hg_T collected in 2008 (Zonta et al., 2018) integrated with observations from 1996 for the industrial canals (Bellucci et al., 2002), subtracting the MeHg concentration estimated from the results of the box-model (Rosati et al., 2020) (Fig. 2b). The seabed is initialized by setting 2% of organic carbon (Zonta et al., 2018) (see Supplementary Material 1.3). Water concentrations have a fast response time and are initialized with spatially homogeneous values.

A mask is applied to the model domain for suppressing bottom shear stress, and thus sediment resuspension, in areas with marshes and seagrass beds. The mask (Fig. 2c) is obtained by integrating data from 2002 for marshes and from 2004 for seagrasses from the public database (Atlante della Laguna, 2011). To evaluate the importance of this model feature, we performed numerical experiments by running the three simulations after removing the mask to quantify the effect on the concentrations of Hg species.

2.4.1. Selection of model parameters

The rate constant for Hg methylation in sediment (k_{met_s}) was set based on site-specific data (Han et al., 2007), while the rate constant for demethylation (K_{Dem_s}) was taken from the Marano-Grado Lagoon (Hines et al., 2012). The rate constants for Hg methylation and demethylation in water were set to values that are in the lower range of observations for other Mediterranean lagoons and estuaries (Monperrus et al., 2007; Sharif et al., 2014). The values for these and other parameters are given in Supplementary Table 11. The published rates of reductive demethylation from field studies in water and sediment of different ecosystems are close to each other (k_{opm_w} = 0.19 d^{-1} in Meadowlands in Schaefer et al. (2004), and k_{opm_s} = 0.25 d^{-1} in the Marano Grado Lagoon in Hines et al. (2012)). Both studies assessed only demethylation, and we applied the same rate constant for Hg^{II} reduction. The rate constants for biological reduction (Lamborg et al., 2021; Monperrus et al., 2007; Lee and Fisher, 2019) and biological oxidation (Poulain et al., 2007) are non site-specific, and those for photochemical transformations are in agreement with previous modeling work on this topic (Soerensen et al., 2010). The values for the partition coefficients of Hg and MeHg to silt ($K_{D_{Hgi-silt}}$) were calculated from k_D estimates for the bulk sediment of the Venice Lagoon (Han et al., 2007; Bloom et al., 2004), and it was assumed that the partition coefficients to POM and DOM are higher than the $K_{D_{Hgi-silt}}$, considering the higher affinity of Hg for organic material than for lithogenic material (Lamborg et al., 2016), which is reflected locally in the higher K_D values estimated for the seston compared to the seafloor sediment (Bloom et al., 2004).

2.4.2. Model corroboration

Modeled concentrations of Hg_T and MeHg in lagoon water were compared against available literature data (Bloom et al., 2004). These data were collected following ultra-clean sampling procedures, analyzed using cold vapor atomic fluorescence spectrometric detection (Bloom and Fitzgerald, 1988), and statistically described by providing average concentrations and standard deviations of Hg and MeHg concentrations in different seasons and lagoon areas (Bloom et al., 2004). Model results were also compared to observations from a similar neighbor ecosystem (the Marano-Grado Lagoon) for variables and processes never assessed in the Venice Lagoon, namely the concentration and volatilization flux of Hg^0.

The data on Hg concentrations in the lagoon sediment (Zonta et al., 2018) used to initialize the model are available at a very high spatial resolution from the 2008 sampling, while the data on Hg species in the lagoon water and at the boundaries cover the period 2001 to 2003 (Bloom et al., 2004). Therefore, we created a non-synoptic setup for model calibration and validation that is representative of the early 2000s. We calibrated the model using water concentrations of SPM and POM measured at 20 lagoon stations in 2005 (Fig. 4), approximately every 15 days (MAV-CVN, 2005), applying meteorological forcings for 2005 which is considered representative of the early 2000s as it relates to the behavior of wind fields in the lagoon (Alpaos et al., 2013). After calibration, the model was validated against concentrations of Hg species in the lagoon water.

To perform calibration, we run a set of simulations (Supplementary Table 14) varying the critical threshold for erosion parameter (τ_{ce}), which regulates sediment resuspension, in a range spanning from 0.45 to 0.7 (Amos et al., 2010). We selected the simulation with the best performances (Supplementary Table 15) based on the statistics reported in Supplementary Equations 107–111 and ran two additional simulations in which the parameter τ_{ce} was perturbed by ±10% to account for uncertainty. Current Hg dynamics in the Venice lagoon were explored by simulating 2019 and 2020. The two years were simulated separately maintaining the same boundary conditions to assess interannual variability, while continuous biannual simulations were run to perform sensitivity analysis. This was done by varying all the parameters related to Hg dynamics, as well as the concentrations of Hg species at the model boundaries (rivers, sea, and atmosphere) by ±50%, as the observational ranges and uncertainty are large enough to justify such variations. Indeed, a general decrease in Hg concentrations in the atmosphere (Zhang et al., 2016), in river (Stoichev et al., 2022; Amos et al., 2014), and in the water of the Mediterranean Sea (Cossa et al., 2020) has been observed in Europe from the 1990s to the early 2010s as a result of emission control measures.

3. Results and discussion

3.1. Data model comparison

The seasonal fluctuations of Hg and MeHg concentrations in the water of the northern lagoon, which were determined in 2001–2003 by Bloom et al. (2004) (Section 2.4.2), were compared with the model results of the early 2000s simulation (Fig. 3). In winter, the modeled Hg_T concentrations are very close to the observations, with a relative error η = 18%. In spring and summer, and to a lesser extent in fall, the field data show an increase in Hg_T concentration that is not captured by the model (η is 48% in summer and about 30% in spring and fall). This dynamic could be attributed to the seasonal increase in anthropogenic activities such as shipping, which intensifies the resuspension of particles from the seabed and the associated mercury (Bloom et al., 2004). Since anthropogenic sediment resuspension is not considered in the model, water concentrations of SPM (Fig. 4) and mercury (Fig. 3a) are underestimated in summer, while the deviation is much smaller in the other seasons. The model performance in reproducing the observed concentrations of SPM (Supplementary Table 15) are comparable to those obtained with other sediment models for the Venice Lagoon (Carniello et al., 2012) and other tidal environments (Winter, 2007). Most of the mismatch with the observations is due to the underestimation of SPM concentrations in summer in the shallow areas of the northern lagoon and in November at a few stations (B7, B9, B17, and C06) in relative proximity to river mouths (Supplementary Figures 4 and 5). The latter is likely due to a sharp increase in river flooding, and consequently, in the concentrations and loadings of SPM, following heavy rainfalls that occurred in October and November 2005, which is not represented in the model boundary conditions. Modeled and observed SPM concentrations are poorly correlated when considering

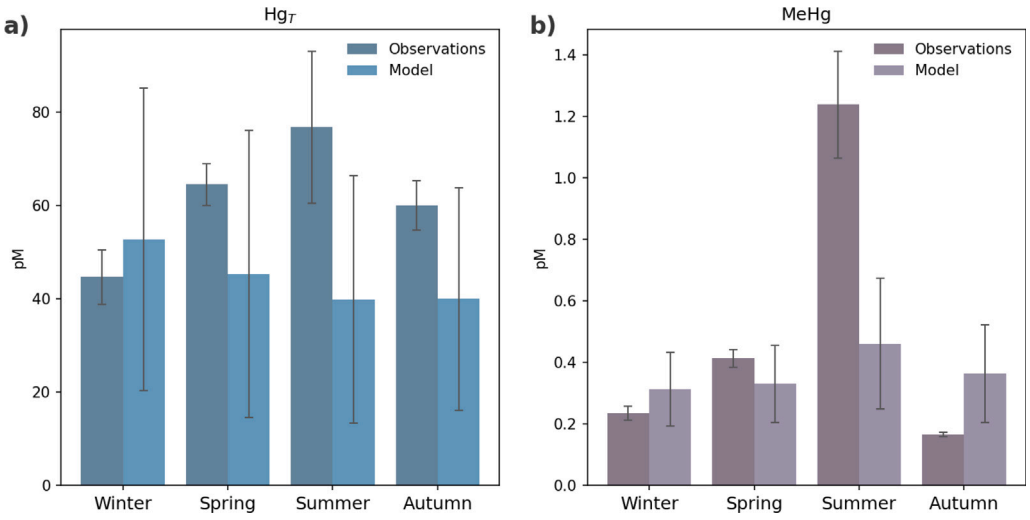

Fig. 3. Comparison between modeled and observed seasonal concentrations (averages and S.D.) of Hg_T and MeHg. Field data (Bloom et al., 2004) were sampled in 2001–2003 at eight stations of the northern lagoon (Supplementary Figure 4), whilst model outputs were extracted at eight nodes corresponding to the sampling stations from the simulation representative of early 2000s.

each point at each station, but the correlation improves (r = 0.44–0.58, $p < 0.05$) when the annual average of each station is considered, indicating the ability of the model to capture spatial variability.

Modeled MeHg concentrations in water are close to observations in winter and spring (with η 33% and 20%, respectively) but underestimate summer values by 62% (the absolute error is 0.77 pM) (Fig. 3b). On the other hand, fall concentrations tend to be overestimated by 120% (with an absolute error of 0.19 pM). We tested different values for the Hg methylation Q-factor (i.e., the coefficient used to parameterize the temperature sensitivity of the reaction — see Supplementary Tables 5 and 11) in a range of 1.5–10 (not shown), and since none of the tests resulted in an improved agreement between modeled and observed MeHg concentrations, we concluded that tuning the Q-factor was not sufficient to reproduce the large variability of MeHg concentrations observed in the field. Conversely, coupling Hg processes with biogeochemical models that resolve plankton, carbon, and nutrient dynamics appears to be a promising way to improve understanding of the interconnected processes that lead to MeHg production (Zhang et al., 2020; Rosati et al., 2022; Bieser et al., 2023; Soerensen et al., 2016). Nonetheless, the lack of mechanistic understanding of Hg methylation/demethylation processes limits the ability of the models to reproduce the observed maxima of MeHg concentrations. Further efforts are needed to ameliorate our ability to predict MeHg concentrations in marine and coastal areas, including better characterization of spatial and temporal variability of fluxes and concentrations in the field.

The spatial distributions of Hg species concentrations in lagoon water (Fig. 5) reflect the sediment contamination gradient with the highest concentrations near the historical Hg sources and the lowest in the southern lagoon. This figure agrees well with field observations (Bloom et al., 2004) indicating much higher concentrations in the northern water (74 ± 3.3 pM of Hg_T and 0.35 ± 0.01 pM of MeHg, up to 145 and 1 pM in wetlands) than in the southern waters (15.7 ± 0.85 pM of Hg_T and 0.13 ± 0.01 pM of MeHg).

However, the spatial–temporal distributions of inorganic Hg^{II} in water are only weakly correlated to water MeHg (r = 0.35) and Hg^0 (r = 0.29) due to the different dynamics governing their fate and transport. Model results provide a first estimate of Hg^0 concentrations (Fig. 5), which have never been assessed in the field. Predicted levels are comparable to those measured in the contaminated Marano-Grado lagoon (Northern Adriatic Sea, Mediterranean Sea) (Emili et al., 2012; O'Driscoll et al., 2019). The modeled volatilization flux of Hg^0 is also comparable to available estimates for the Marano-Grado lagoon (51–80 ng m^{-2} h^{-1}, (Floreani et al., 2019) and the Augusta Bay (36–72 ng m^{-2} h^{-1}, (Bagnato et al., 2013) which is another contaminated Mediterranean bay located in the Ionian Sea. The modeled flux is on average 51 ± 29 ng m^{-2} h^{-1} (about 254 ± 144 pmol m^{-2} h^{-1}) for the early 2000s simulation, and lower in 2019 (49 ± 28 ng m^{-2} h^{-1}) and 2020 (35 ± 20 ng m^{-2} h^{-1}), when Hg^0 concentrations are also lower.

3.2. Spatial and temporal variability of Hg species concentrations

The importance of interannual variability was explored by simulating three years (Fig. 5 and Supplementary Figures 6 and 7) with different meteo-climatic and oceanographic conditions (Supplementary Figures 2 and 3). Different drivers control the evolution of the Hg state variables, resulting in contrasting dynamics for the three mercury species. The concentrations of the inorganic Hg species were highest and the MeHg concentrations lowest in the early 2000s simulation. This simulation is characterized by an intermediate river inflow and the highest wind speed, which trigger sediment resuspension that also causes the highest water concentrations of silt and POM. By contrast, modeled MeHg concentrations were highest in 2020, a year with minimal river inflow but higher temperatures than in the early 2000s and an intermediate wind speed. In 2019, wind speed and sediment resuspension were lower than in the other years, but river inflow was abundant, so concentrations of inorganic Hg species remained higher than in 2020.

The MeHg concentrations modeled for 2019 were slightly lower than in 2020, but higher than in the early 2000s, as the warm temperatures partially offset the lower input from sediment resuspension. The high river inflow of 2019 also contributes to maintain the MeHg pool in the water, but the sensitivity analysis showed a weaker effect on MeHg than on inorganic Hg species (Section 3.3), while the correlation with water temperature is stronger for MeHg (0.37, $p < 0.05$) than for other Hg species (0.32 for Hg^0 and 0.29 for Hg^{II}, $p < 0.05$). On the other hand, the distributions of inorganic Hg species correlate more strongly with SPM (r = 0.21 for Hg^{II} and 0.18 for Hg^0, $p < 0.05$) than MeHg (r = 0.16, $p < 0.05$).

The different fate of Hg^{II} and MeHg in the lagoon water becomes even clearer by analyzing the spatial distribution of the modeled concentrations on days with different hydrodynamic conditions. On a day with high turbulence (Fig. 6a), the water concentrations of Hg^{II}, silt and POM_{ref} are noticeably higher than on days with medium (Fig. 6b) and low (Fig. 6c) turbulence. This response occurs mainly in the northern lagoon, as in the southern lagoon more areas of marshes and

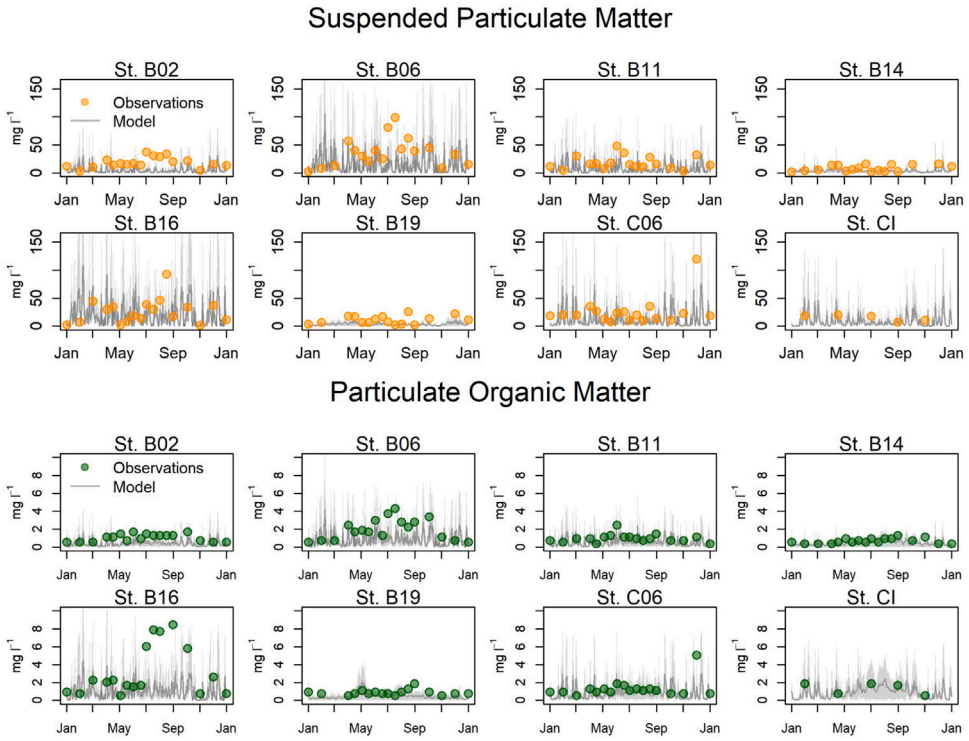

Fig. 4. Yearly evolution of modeled concentrations of SPM (upper panel, as the sum of silt$_w$, POM$_{R(w)}$, and POM$_{L(w)}$) and POM (lower panel) at selected stations of the Venice Lagoon gray lines and shaded areas are the average, minimum, and maximum of the three simulations ensamble compared with observations (MAV-CVN, 2005). The location of the sampling stations is indicated in Supplementary Figure 4.

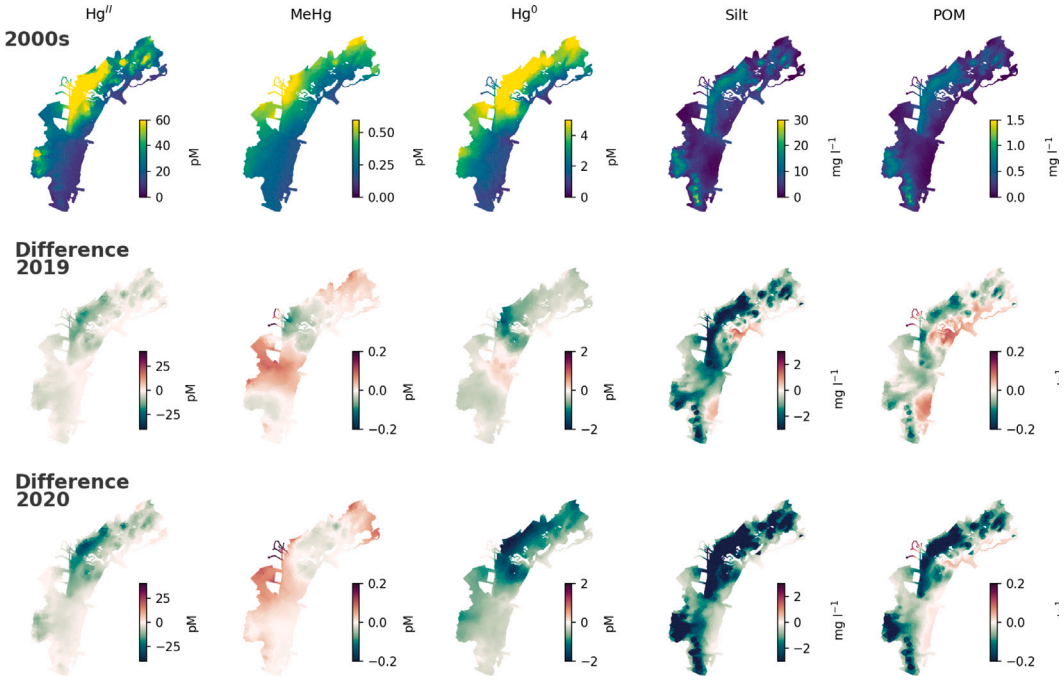

Fig. 5. Maps showing the average spatial distributions of the modeled state variables (Hg^{II}, MeHg and Hg^0, silt and POM) in the lagoon water for the simulation of the early 2000s (upper panels) and the concentration variations obtained by applying meteorological forcings for 2019 (intermediate panels) and 2020 (lower panels).

seagrass (Fig. 2c) limit the amount of sediment and Hg that is resuspended. MeHg concentrations are less variable and remain relatively high in low turbulence, so they are decoupled from the distribution of Hg^{II} and suspended sediment (Fig. 6a–c). MeHg is less effectively scavenged than Hg^{II} and tends to remain in the water longer due to its lower affinity for inorganic particles, whereas Hg^{II}, which is more closely associated with SPM, tends to settle faster under calm conditions.

The MeHg and Hg^0 concentrations in water show a consistent seasonality over the three simulated years (Supplementary Figure 7), with maximum values in summer and spring respectively. Hg^{II} concentrations do not show a clear pattern and tend to be higher either in

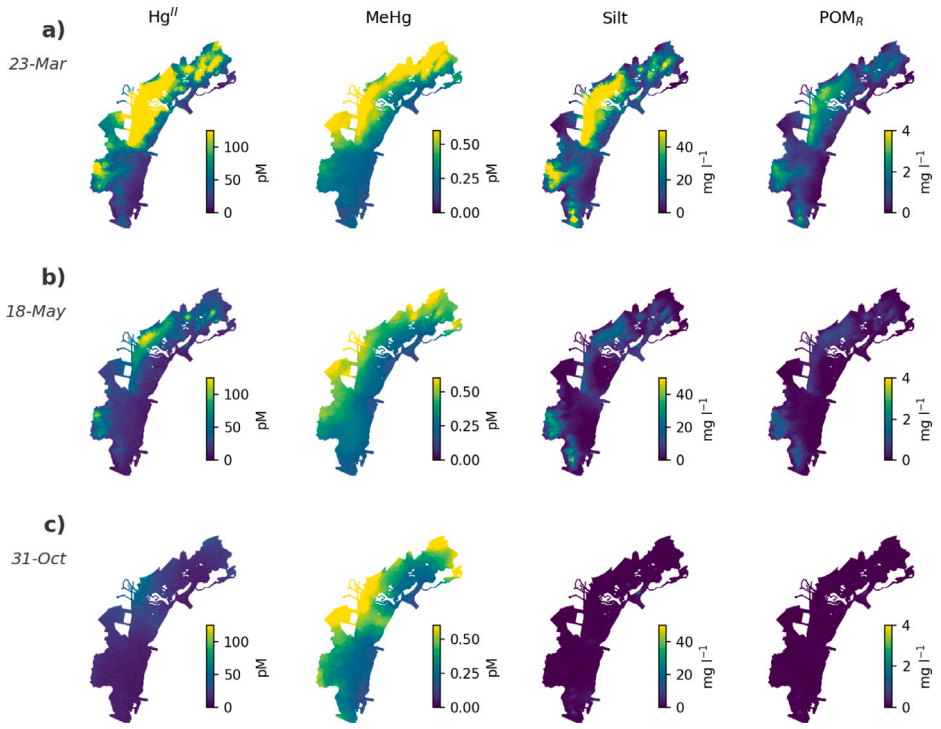

Fig. 6. Modeled spatial distributions of concentrations of Hg^{II}, MeHg, silt, and POM_{ref} during days with contrasting meteorological and hydrodynamic conditions. (a) 23 March 2020, average wind speed = 8 m s^{-1}, (b) 18 May 2020, average wind speed = 5 m s^{-1}, (c) 31 October 2020, average wind speed = 2 m s^{-1}.

winter or spring, depending on wind speeds in combination with river inflows.

3.3. Model sensitivity

The sheltering effect of marshes and seagrasses on the seafloor had a marked effect on the modeled dynamics of Hg species. The numerical experiments carried out by removing the mask (Fig. 2c) that hinders sediment resuspension in correspondence of these benthic features resulted in an increase of water concentrations of all Hg species (on average, 190% for Hg^{II}, 22% for MeHg, and 17% for Hg^0).

The sensitivity analysis (Supplementary Table 16) confirmed that processes associated with sediment resuspension have a major influence on the concentrations of Hg species. Increasing the parameter τ_{ce} by 50% and thus reducing sediment resuspension led to a decrease in water concentrations of Hg^{II}, Hg^0 and MeHg by 76%, 68%, and 12% respectively and to a moderate increase in sediment concentrations of the three species (0.3%–3%). When a negative variation is applied to τ_{ce}, the water concentrations of Hg^{II} increase by 59%, but the strong erosion leads to a noticeable decrease in the MeHg pool in the sediment (41%), which also causes a reduction in water concentrations (39%) after an initial increase. This unexpected behavior was caused by an imbalance in the system, as this simulation reproduced an extreme dynamic, unlikely to happen in the field, where resuspension never ceased and out-competed deposition leading to a severe increase in SPM concentrations (76 mg l^{-1} on average) compared to the baseline simulation (7 mg l^{-1} on average). In the first months of simulation, a remarkable remobilization of all Hg species from the sediment occurred causing a spike in water concentrations and consequently increasing the export at the lagoon boundaries (i.e., removing mass of Hg). After about four months of continuous erosion, the sediment pool of Hg and MeHg was significantly reduced compared to the initial state, so that the resuspension in the following months acted on “cleaner” sediment and could only mobilize a limited amount of Hg species. In addition, the high SPM concentrations reduced the fraction of bioavailable dissolved Hg species in the water, which hindered the transformation processes in the water column and caused a reduction in Hg^0 concentrations (55%) that was even greater than that of MeHg. In terms of boundary conditions, the largest change in modeled concentrations results from the increase in seawater concentrations of Hg species, which causes a concentration increase of about 10% for Hg^{II} and Hg^0 and about 4% for MeHg. However, assuming a 50% decrease in seawater concentrations, the modeled water concentrations only decrease by 2%–5%. A decrease in river concentrations of Hg^{II} leads to variations of less than 2% for all Hg species, while a decrease in river MeHg concentrations causes a 0.6% decrease in MeHg concentrations. The Hg concentration in the atmospheric boundary has comparable effects to the river boundary. For most processes, the results of the sensitivity analysis are fairly symmetrical between increases and decreases, so hereon only the positive variations are discussed. Variations in the partition coefficients of Hg^{II} have remarkable effects on the modeled concentrations because they regulate the tendency of Hg to bind with inorganic solids, which affects both its transport and its availability for transformations. Increasing the parameter $K_{D-\mathrm{Hg}-silt}$ by 50% causes a decrease in the water concentrations of Hg^{II}, Hg^0 and MeHg by 11% 21% and 6% respectively. In this simulation, more Hg^{II} is retained in the sediment (+1%), but its lower bioavailability leads to a decrease in the concentrations of MeHg in the sediment (−6%) and Hg^0 in the pore water (−38%). On the other hand, the parameter $K_{D-\mathrm{Hg}-DOC}$ contributes to keeping Hg^{II} in the dissolved pool, which favors an increase in water concentrations of all Hg species. Perturbing the same parameters for MeHg (i.e. $K_{D_{\mathrm{MeHg}-silt}}$ and $K_{D_{\mathrm{MeHg}-DOC}}$) leads to fluctuations in MeHg concentrations of about ±10% in water and ±2% in sediment and negligible effects on the other Hg species. For the transformation of Hg species, the strongest effects on the modeled concentrations are given by photochemical reduction and oxidation, which lead to an increase of 32% and a decrease of 25% of the Hg^0 concentrations in water, respectively. An increase in the rate constant for methylation of Hg in water leads to an increase of 10% in MeHg concentrations in water and a modest increase (about 1.5%) in concentrations in sediment, while an increase in the rate constant for demethylation in water leads to an increase of 2.5% in MeHg in water, which is due to a

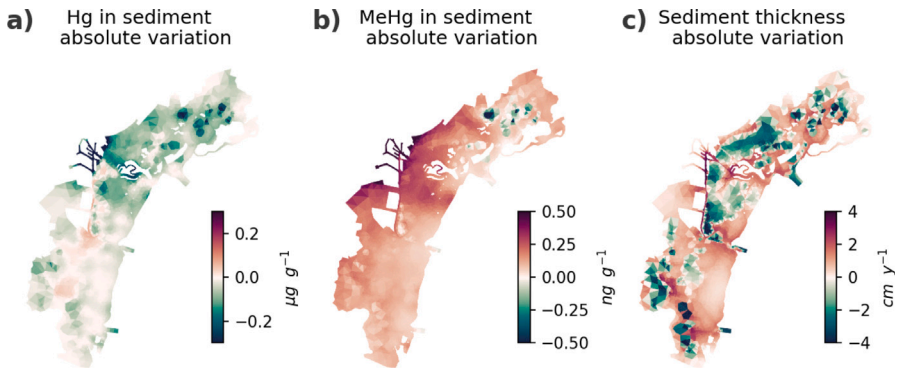

Fig. 7. Variations over one year of simulation of sediment concentrations of (a) Hg^{II} (μg g^{-1} y^{-1}) and (b) MeHg (ng g^{-1} y^{-1}). Panel (c) shows the morphological evolution of the seabed (cm y^{-1}).

small increase (0.01%) in the concentrations of inorganic Hg available for methylation. Perturbation of the rate constant for Hg methylation in sediment has a greater effect on MeHg concentrations in sediment (+1.4%) than perturbation of the demethylation rate constant (−0.6%). The microbial mercury resistance mediated by the mer operon has a strong effect on the Hg^0 content in pore water (30%) and a negligible effect on the concentrations of inorganic Hg, while the impact on MeHg in water (0.4%) is in the order of magnitude of that of riverine and atmospheric inputs.

3.4. Seabed dynamics

The modeled morphological evolution of the seabed over the course of a year (Fig. 7c) shows that resuspension exceeds deposition in large areas of the northern lagoon leading to seabed erosion. This agrees reasonably well with the erosion rates estimated with a retrospective analysis of the bathymetric changes of the lagoon, which roughly correspond to a net sediment loss towards the sea of 0.8 Mm^3 y^{-1} (Sarretta et al., 2010).

Net erosion of the seabed in the lagoon areas with the highest initial concentrations (Fig. 2a) led to an overall decrease in Hg^{II} concentrations in the sediments over a year (Fig. 7a) of up to −0.3 μg g^{-1}, which can be attributed to the resuspension and export of contaminated sediment particles. However, Hg is also redistributed within the lagoon, and sediment Hg^{II} concentrations increased slightly in some areas of the southern lagoon with low initial concentrations. In contrast, sediment MeHg concentrations are predicted to increase slightly independently of sediment erosion (up to 0.5 ng g^{-1}) as long as sufficient Hg^{II} remains available for methylation. The general decrease in inorganic Hg concentrations is conceptually consistent with strong erosion processes in some lagoon areas and sediment losses towards the sea (Sarretta et al., 2010) in conjunction with the post-industrial decrease in Hg loading from the catchment due to the closure of industrial plants (Rosati et al., 2022). Observations from sediment cores also confirm the loss of fine particles from the upper sediment layers and a progressive homogenization of Hg_T concentrations in the surface sediment of the lagoon (Zonta et al., 2018).

4. Conclusions

We developed a new tool for the fate and transport of Hg species in coastal environments by coupling Hg biogeochemistry with hydrodynamics and sediment dynamics. The model was used to simulate Hg dynamics in the Venice lagoon with high spatial resolution under different meteo-climatic conditions. High water concentrations of Hg^{II} (up to 80 pM) and MeHg (up to 1.0 pM) were simulated, which is consistent with observations from previous studies in this lagoon and other contaminated sites. However, the study area is characterized by a strong spatio-temporal variability of Hg species, especially inorganic oxidized Hg, which is the most affected by the benthic-pelagic coupling and the impulsive nature of the sediment resuspension.

The assumption of improved water quality of the river and marine boundaries in recent years, simulated by a 50% reduction in Hg species concentrations, results in a small variation of Hg species concentrations within the lagoon (<5% for each boundary). The sensitivity analysis also showed that in addition to sediment dynamics, Hg partitioning, Hg concentrations at the marine boundaries, and Hg methylation dynamics should be better constrained by observations to reduce the uncertainty of the model results. Microbial resistance has a minor impact on oxidized Hg, but contributes to lowering environmental concentrations of MeHg.

The local dynamics of seabed erosion likely lead to the mobilization of inorganic Hg from the sediment, especially from the most contaminated areas, and to its export and redistribution throughout the lagoon. Such dynamics can be expected at polluted sites characterized by erosion or strong sediment resuspension.

The results highlight the importance of considering sediment transport dynamics in biogeochemical models of Hg cycling in shallow contaminated environments and suggest a crucial role of benthic vegetation in lowering water levels of Hg species in the Venice Lagoon and similar ecosystems. Maintaining the integrity of benthic morphology and vegetation can significantly improve water quality by limiting the resuspension of sediments, with limited effects on sediment Hg concentrations.

CRediT authorship contribution statement

Ginevra Rosati: Writing – review & editing, Writing – original draft, Visualization, Validation, Software, Methodology, Investigation, Formal analysis, Data curation, Conceptualization. **Cosimo Solidoro:** Writing – review & editing, Writing – original draft, Validation, Supervision, Resources, Project administration, Methodology, Funding acquisition, Conceptualization. **Célia Laurent:** Writing – review & editing, Writing – original draft, Visualization, Validation, Software, Methodology, Data curation. **Leslie Aveytua Alcázar:** Writing – review & editing, Data curation, Methodology. **Georg Umgiesser:** Writing – review & editing, Validation, Software. **Donata Canu:** Writing – review & editing, Writing – original draft, Validation, Supervision, Software, Resources, Project administration, Methodology, Investigation, Funding acquisition, Data curation, Conceptualization.

Declaration of competing interest

The authors declare the following financial interests/personal relationships which may be considered as potential competing interests: Donata Canu reports financial support was provided by Provveditorato for the Public Works of Veneto, Trentino Alto Adige, and Friuli Venezia Giulia, provided through the concessionary of State Consorzio Venezia

Nuova and coordinated by CORILA. Donata Canu, Cosimo Solidoro reports financial support was provided by Government of Italy Ministry of University and Research. Donata Canu reports financial support was provided by Ministry of Infrastructure and Transport.

Data availability

The code is available on the Zenodo repository with DOI:10.5281/zenodo.11933313, https://zenodo.org/records/11933313.

Acknowledgments

We thank Dr. R. Zonta for sharing the dataset on sediment concentrations of total Hg, and Dr. L. Carniello and Dr. M. Pivato for insightful discussions on sediment dynamics in the Venice Lagoon. This work was supported by the project Venezia2021 of Provveditorato for the Public Works of Veneto, Trentino Alto Adige, and Friuli Venezia Giulia, provided through the concessionary of State Consorzio Venezia Nuova and coordinated by CORILA. This work was partially supported by the Danubius-RI European Research Infrastructure and the RETURN Extended Partnership that received funding the European Union Next-GenerationEU (National Recovery and Resilience Plan – NRRP, Mission 4, Component 2, Investment 1.3 – D.D. 1243 2/8/2022, PE0000005).

Appendix A. Supplementary data

Supplementary material related to this article can be found online at https://doi.org/10.1016/j.watres.2024.121965.

References

Acquavita, A., Covelli, S., Emili, A., Berto, D., Faganeli, J., Giani, M., Horvat, M., Koron, N., Rampazzo, F., 2012. Mercury in the sediments of the Marano and Grado Lagoon (northern adriatic sea): Sources, distribution and speciation. Estuar. Coast. Shelf Sci. 113 (February), 20–31. http://dx.doi.org/10.1016/j.ecss.2012.02.012.

Alpaos, A.D., Carniello, L., Rinaldo, A., 2013. Statistical mechanics of wind wave-induced erosion in shallow tidal basins : Inferences from the Venice Lagoon, 40, 3402–3407. http://dx.doi.org/10.1002/grl.50666.

Amos, H.M., Jacob, D.J., Kocman, D., Horowitz, H.M., Zhang, Y., Dutkiewicz, S., Horvat, M., Corbitt, E.S., Krabbenhoft, D.P., Sunderland, E.M., 2014. Global biogeochemical implications of mercury discharges from rivers and sediment burial. Environ. Sci. Technol. 48 (16), 9514–9522. http://dx.doi.org/10.1021/es502134t.

Amos, C.L., Umgiesser, G., Ferrarin, C., Thompson, C.E., Whitehouse, R.J., Sutherland, T.F., Bergamasco, A., 2010. The erosion rates of cohesive sediments in Venice Lagoon, Italy. Cont. Shelf Res. 30, 859–870. http://dx.doi.org/10.1016/j.csr.2009.12.001.

Atlante della Laguna, 2011. Atlante della laguna. https://www.atlantedellalaguna.it/. Online; (Accessed 23 June 2023).

Aveytua-Alcazar, L., Melaku Canu, D., Camacho-Ibar, V., Solidoro, C., 2020. Changes in upwelling regimes in a mediterranean-type lagoon: A model application. Ecol. Model. 418, 108908. http://dx.doi.org/10.1016/j.ecolmodel.2019.108908.

Avnimelech, Y., Ritvo, G., Meijer, L.E., Kochba, M., 2001. Water content, organic carbon and dry bulk density in flooded sediments. Aquac. Eng. 25 (1), 25–33. http://dx.doi.org/10.1016/S0144-8609(01)00068-1.

Bagnato, E., Sproveri, M., Barra, M., Bitetto, M., Bonsignore, M., Calabrese, S., Di Stefano, V., Oliveri, E., Parello, F., Mazzola, S., 2013. The sea–air exchange of mercury (hg) in the marine boundary layer of the augusta basin (southern Italy): Concentrations and evasion flux. Chemosphere 93, 2024–2032. http://dx.doi.org/10.1016/j.chemosphere.2013.07.025.

Balcom, P.H., Schartup, A.T., Mason, R.P., Chen, C.Y., 2015. Sources of water column methylmercury across multiple estuaries in the northeast U.S.. Mar. Chem. 177, 721–730. http://dx.doi.org/10.1016/j.marchem.2015.10.012.

Baldi, F., Gallo, M., Marchetto, D., Fani, R., Maida, I., Horvat, M., Fajon, V., Zizek, S., Hines, M., 2012. Seasonal mercury transformation and surficial sediment detoxification by bacteria of Marano and Grado Lagoons. Estuar. Coast. Shelf Sci. 113, 105–115. http://dx.doi.org/10.1016/j.ecss.2012.02.008.

Banchi, E., Corre, E., Negro, P.D., Celussi, M., Malfatti, F., 2023. Genome-resolved metagenomics of Venice Lagoon surface sediment bacteria reveals high biosynthetic potential and metabolic plasticity as successful strategies in an impacted environment. Mar. Life Sci. Technol. http://dx.doi.org/10.1007/s42995-023-00192-z.

Banchi, E., Negro, P.D., Celussi, M., Malfatti, F., 2021. Sediment features and human activities structure the surface microbial communities of the Venice Lagoon. Front. Mar. Sci. 8, http://dx.doi.org/10.3389/fmars.2021.762292.

Bandelj, V., Curiel, D., Lek, S., Rismondo, A., Solidoro, C., 2009. Modelling spatial distribution of hard bottom benthic communities and their functional response to environmental parameters. Ecol. Model. 220, 2838–2850. http://dx.doi.org/10.1016/j.ecolmodel.2009.04.024.

Bandelj, V., Socal, G., Park, Y.S., Lek, S., Coppola, J., Camatti, E., Capuzzo, E., Milani, L., Solidoro, C., 2008. Analysis of multitrophic plankton assemblages in the Lagoon of Venice. Mar. Ecol. Prog. Ser. 368, 23–40. http://dx.doi.org/10.3354/meps07565.

Barkay, T., Miller, S.M., Summers, A.O., 2003. Bacterial mercury resistance from atoms to ecosystems. FEMS Microbiol. Rev. 27, 355–384. http://dx.doi.org/10.1016/S0168-6445(03)00046-9.

Bellucci, L.G., Frignani, M., Paolucci, D., Ravanelli, M., 2002. Distribution of heavy metals in sediments of the Venice Lagoon: the role of the industrial area. Sci. Total Environ. 295, 35–49. http://dx.doi.org/10.1016/s0048-9697(02)00040-2.

Bieser, J., Amptmeijer, D.J., Daewel, U., Kuss, J., Soerensen, A.L., Schrum, C., 2023. The 3D biogeochemical marine mercury cycling model MERCY v2.0 – linking atmospheric hg to methylmercury in fish. Geoscientific Model Development 16, 2649–2688. http://dx.doi.org/10.5194/gmd-16-2649-2023.

Bloom, N., Fitzgerald, W.F., 1988. Determination of volatile mercury species at the picogram level by low-temperature gas chromatography with cold-vapour atomic fluorescence detection. Anal. Chim. Acta 208, 151–161. http://dx.doi.org/10.1016/S0003-2670(00)80743-6.

Bloom, N.S., Moretto, L.M., Scopece, P., Ugo, P., 2004. Seasonal cycling of mercury and monomethyl mercury in the Venice Lagoon (Italy). Mar. Chem. 91 (1–4), 85–99. http://dx.doi.org/10.1016/j.marchem.2004.06.002.

Bowman, K.L., Lamborg, C.H., Agather, A.M., 2020. A global perspective on mercury cycling in the ocean. Sci. Total Environ. 710, 136166. http://dx.doi.org/10.1016/j.scitotenv.2019.136166.

Bravo, A.G., Bouchet, S., Tolu, J., Björn, E., Mateos-Rivera, A., Bertilsson, S., 2017. Molecular composition of organic matter controls methylmercury formation in boreal lakes. Nature Commun. 8, 1–9. http://dx.doi.org/10.1038/ncomms14255.

Bravo, A.G., Loizeau, J.L., Bouchet, S., Richard, A., Rubin, J.F., Ungureanu, V.G., Amouroux, D., Dominik, J., 2010. Mercury human exposure through fish consumption in a reservoir contaminated by a chlor-alkali plant: Babeni reservoir (Romania). Environ. Sci. Pollut. Res. 17, 1422–1432. http://dx.doi.org/10.1007/s11356-010-0328-9.

Canu, D.M., Campostrini, P., Riva, S.D., Pastres, R., Pizzo, L., Rossetto, L., Solidoro, C., 2011. Addressing sustainability of clam farming in the Venice Lagoon. Ecol. Soc. 16.

Canu, D., Rosati, G., 2017. Long-term scenarios of mercury budgeting and exports for a mediterranean hot spot (Marano-Grado Lagoon, Adriatic Sea). Estuar. Coast. Shelf Sci. 198, 518–528. http://dx.doi.org/10.1016/j.ecss.2016.12.005.

Carniello, L., Defina, a., D'Alpaos, L., 2012. Modeling sand-mud transport induced by tidal currents and wind waves in shallow microtidal basins: Application to the Venice Lagoon (Italy). Estuar. Coast. Shelf Sci. 102–103, 105–115. http://dx.doi.org/10.1016/j.ecss.2012.03.016.

Carniello, L., Silvestri, S., Marani, M., D'Alpaos, A., Volpe, V., Defina, A., 2014. Sediment dynamics in shallow tidal basins: In situ observations, satellite retrievals, and numerical modeling in the Venice Lagoon. J. Geophys. Res.: Earth Surf. 119 (4), 802–815. http://dx.doi.org/10.1002/2013JF003015.

Chen, C.Y., Borsuk, M.E., Bugge, D.M., Hollweg, T., Balcom, P.H., Ward, D.M., Williams, J., Mason, R.P., 2014. Benthic and pelagic pathways of methylmercury bioaccumulation in estuarine food webs of the northeast United States. PLoS ONE 9 (2), http://dx.doi.org/10.1371/journal.pone.0089305.

Chen, C., Driscoll, C., Lambert, K., Mason, R., Sunderland, E., 2016. Connecting mercury science to policy: from sources to seafood. Rev. Environ. Health 31, 131–135. http://dx.doi.org/10.1515/reveh-2015-0044.

Conaway, C.H., Squire, S., Mason, R.P., Flegal, A.R., 2003. Mercury speciation in the San Francisco Bay estuary. Mar. Chem. 80 (2–3), 199–225. http://dx.doi.org/10.1016/S0304-4203(02)00135-4.

Cossa, D., Knoery, J., Boye, M., Marusczak, N., Thomas, B., Courau, P., Sprovieri, F., 2020. Oceanic mercury concentrations on both sides of the strait of gibraltar decreased between 1989 and 2012. Anthropocene 29, http://dx.doi.org/10.1016/j.ancene.2019.100230.

Cossa, D., Knoery, J., B˘ anaru, D., Harmelin-Vivien, M., Sonke, J.E., Hedgecock, I.M., Bravo, A.G., Rosati, G., Canu, D., Horvat, M., Sprovieri, F., Pirrone, N., Heimbürger-Boavida, L.-E., 2022. Mediterranean mercury assessment 2022: An updated budget, health consequences, and research perspectives. Environ. Sci. Technol. http://dx.doi.org/10.1021/acs.est.1c03044.

Cossarini, G., Libralato, S., Salon, S., Gao, X., Giorgi, F., Solidoro, C., 2008. Downscaling experiment for the Venice Lagoon. II. Effects of changes in precipitation on biogeochemical properties. Clim. Res. 38, 43–59. http://dx.doi.org/10.3354/cr00758.

Critto, A., Carlon, C., Marcomini, A., 2005. Screening ecological risk assessment for the benthic community in the Venice Lagoon (Italy). Environ. Int. 31, 1094–1100. http://dx.doi.org/10.1016/j.envint.2005.05.046.

Dominik, J., Tagliapietra, D., Bravo, A.G., Sigovini, M., Spangenberg, J.E., Amouroux, D., Zonta, R., 2014. Mercury in the food chain of the Lagoon of Venice, Italy. Mar. Pollut. Bull. 88 (1–2), 194–206. http://dx.doi.org/10.1016/j.marpolbul.2014.09.005.

Emili, A., Acquavita, A., Koron, N., Covelli, S., Faganeli, J., Horvat, M., Žižek, S., Fajon, V., 2012. Benthic flux measurements of hg species in a northern adriatic lagoon environment (Marano and Grado Lagoon, Italy). Estuar. Coast. Shelf Sci. 113, 71–84. http://dx.doi.org/10.1016/j.ecss.2012.05.018.

Emili, A., Carrasco, L., Acquavita, A., Covelli, S., 2014. A laboratory-incubated redox oscillation experiment to investigate Hg fluxes from highly contaminated coastal marine sediments (Gulf of Trieste, Northern Adriatic Sea). Environ. Sci. Pollut. Res. Int. 21, 4124–4133. http://dx.doi.org/10.1007/s11356-013-2225-5.

Ferrarin, C., Umgiesser, G., Bajo, M., Bellafiore, D., Pascalis, F.D., Ghezzo, M., Mattassi, G., Scroccaro, I., 2010. Hydraulic zonation of the lagoons of Marano and Grado, Italy. A modelling approach. Estuar. Coast. Shelf Sci. 87, 561–572. http://dx.doi.org/10.1016/j.ecss.2010.02.012.

Floreani, F., Acquavita, A., Petranich, E., Covelli, S., 2019. Diurnal fluxes of gaseous elemental mercury from the water-air interface in coastal environments of the northern Adriatic Sea. Sci. Total Environ. 668, 925–935. http://dx.doi.org/10.1016/j.scitotenv.2019.03.012.

Gibičar, D., Horvat, M., Logar, M., Fajon, V., Falnoga, I., Ferrara, R., Lanzillotta, E., Ceccarini, C., Mazzolai, B., Denby, B., Pacyna, J., 2009. Human exposure to mercury in the vicinity of chlor-alkali plant. Environ. Res. 109 (4), 355–367. http://dx.doi.org/10.1016/j.envres.2009.01.008.

Guédron, S., Huguet, L., Vignati, D.A.L., Liu, B., Gimbert, F., Ferrari, B.J.D., Zonta, R., Dominik, J., 2012. Tidal cycling of mercury and methylmercury between sediments and water column in the Venice Lagoon (Italy). Mar. Chem. 130–131, 1–11. http://dx.doi.org/10.1016/j.marchem.2011.12.003.

Han, S., Obraztsova, A., Pretto, P., Choe, K.-Y., Gieskes, J., Deheyn, D.D., Tebot, B.M., 2007. Biogeochemical factors affecting mercury methylation in sediments of the Venice Lagoon, Italy. Environ. Toxicol. Chem. / SETAC 26, 655–663. http://dx.doi.org/10.1897/06-392R.1.

Hines, M.E., Poitras, E.N., Covelli, S., Faganeli, J., Emili, A., Žižek, S., Horvat, M., 2012. Mercury methylation and demethylation in Hg-contaminated lagoon sediments (Marano and Grado Lagoon, Italy). Estuar. Coast. Shelf Sci. 113, 85–89. http://dx.doi.org/10.1016/j.ecss.2011.12.021.

Hollweg, T., Gilmour, C.C., Mason, R.P., 2009. Methylmercury production in sediments of Chesapeake Bay and the mid-atlantic continental margin. Mar. Chem. 114 (3–4), 86–101. http://dx.doi.org/10.1016/j.marchem.2009.04.004.

Hsu-Kim, H., Eckley, C.S., Achá, D., Feng, X., Gilmour, C.C., Jonsson, S., Mitchell, C.P., 2018. Challenges and opportunities for managing aquatic mercury pollution in altered landscapes. Ambio 47, 141–169. http://dx.doi.org/10.1007/s13280-017-1006-7.

ISPRA Ambiente, 2023. ISPRA ambiente. https://www.venezia.isprambiente.it/. Online; (Accessed 23 June 2023).

Kotnik, J., Horvat, M., Ogrinc, N., Fajon, V., Žagar, D., Cossa, D., Sprovieri, F., Pirrone, N., 2015. Mercury speciation in the Adriatic sea. Mar. Pollut. Bull. 96, 136–148. http://dx.doi.org/10.1016/j.marpolbul.2015.05.037.

Lamborg, C.H., Hammerschmidt, C.R., Bowman, K.L., 2016. An examination of the role of particles in oceanic mercury cycling. Phil. Trans. R. Soc. A 374 (2081), 20150297. http://dx.doi.org/10.1098/rsta.2015.0297.

Lamborg, C.H., Hansel, C.M., Bowman, K.L., Voelker, B.M., Marsico, R.M., Oldham, V.E., Swarr, G.J., Zhang, T., Ganguli, P.M., 2021. Dark reduction drives evasion of mercury from the ocean. Front. Environ. Chem. 2, http://dx.doi.org/10.3389/fenvc.2021.659085.

Lee, C.S., Fisher, N.S., 2019. Microbial generation of elemental mercury from dissolved methylmercury in seawater. Limnol. Oceanogr. 64 (2), 679–693. http://dx.doi.org/10.1002/lno.11068.

Liu, M., Mason, R.P., Vlahos, P., Whitney, M.M., Zhang, Q., Warren, J.K., Wang, X., Baumann, Z., 2023. Riverine discharge fuels the production of methylmercury in a large Temperate Estuary. Environ. Sci. Technol. 57, 13056–13066. http://dx.doi.org/10.1021/acs.est.3c00473.

Liu, M., Zhang, Q., Maavara, T., Liu, S., Wang, X., Raymond, P.A., 2021. Rivers as the largest source of mercury to coastal oceans worldwide. Nat. Geosci. http://dx.doi.org/10.1038/s41561-021-00793-2.

Marani, M., Da Lio, C., D'Alpaos, A., 2013. Vegetation engineers marsh morphology through multiple competing stable states. Proc. Natl. Acad. Sci. USA 110, 3259–3263. http://dx.doi.org/10.1073/pnas.1218327110.

Marcomini, A., Pojana, G., Sfriso, A., Alonso, J.M.Q., 2000. Behavior of anionic and nonionic surfactants and their persistent metabolites in the Venice Lagoon, Italy. Environ. Toxicol. Chem. 19, 2000–2007. http://dx.doi.org/10.1002/etc.5620190807.

Marvin-DiPasquale, M., Agee, J., McGowan, C., Oremland, R.S., Thomas, M., Krabbenhoft, D., Gilmour, C.C., 2000. Methyl-mercury degradation pathways: A comparison among three mercury-impacted ecosystems. Environ. Sci. Technol. 34, 4908–4916. http://dx.doi.org/10.1021/es0013125.

Mason, R.P., Buckman, K.L., Seelen, E.A., Taylor, V.F., Chen, C.Y., 2023. An examination of the factors influencing the bioaccumulation of methylmercury at the base of the estuarine food web. Sci. Total Environ. 886, http://dx.doi.org/10.1016/j.scitotenv.2023.163996.

Matsuyama, A., Yano, S., Taniguchi, Y., Kindaichi, M., Tada, A., Wada, M., 2021. Trends in mercury concentrations and methylation in Minamata Bay, Japan, between 2014 and 2018. Mar. Pollut. Bull. 173, http://dx.doi.org/10.1016/j.marpolbul.2021.112886.

MAV-CVN, 1999. Mappatura dell'inquinamento sei Fondali Lagunari. Report Finale - Mapping of Pollution of the Lagoon Sediment. Final Report (in italian). Technical Report.

MAV-CVN, 2005. Attività di Monitoraggio Ambientale della Laguna di Venezia. Esecutivo del II Stralcio Triennale (2002 - 2005) - Environmental Monitoring in the Venice Lagoon. Triennial Report (2002 - 2005) (in italian). Technical Report, p. 91.

Melaku Canu, D., Aveytua-Alcázar, L., Camacho-Ibar, V.F., Querin, S., Solidoro, C., 2016. Hydrodynamic properties of San Quintin Bay, Baja California: Merging models and observations. Mar. Pollut. Bull. 108 (1), 203–214. http://dx.doi.org/10.1016/j.marpolbul.2016.04.030.

Melaku Canu, D., Rosati, G., Solidoro, C., Heimbürger, L.-E., Acquavita, A., 2015. A comprehensive assessment of the mercury budget in the Marano–Grado Lagoon (Adriatic Sea) using a combined observational modeling approach. Mar. Chem. 177, 742–752. http://dx.doi.org/10.1016/j.marchem.2015.10.013.

Melaku Canu, D., Solidoro, C., Umgiesser, G., 2003. Modelling the responses of the Lagoon of Venice ecosystem to variations in physical forcings. Ecol. Model. 170, 265–289. http://dx.doi.org/10.1016/j.ecolmodel.2003.07.004.

Micheletti, C., Critto, A., Carlon, C., Marcomini, A., 2004. Ecological risk assessment of persistent toxic substances for the clam tapes philipinarum in the Lagoon of Venice, Italy. Environ. Toxicol. Chem. 23, 1575–1582. http://dx.doi.org/10.1897/03-331.

Monperrus, M., Tessier, E., Amouroux, D., Leynaert, A., Huonnic, P., Donard, O.F.X., 2007. Mercury methylation, demethylation and reduction rates in coastal and marine surface waters of the Mediterranean sea. Mar. Chem. 107, 49–63. http://dx.doi.org/10.1016/j.marchem.2007.01.018.

Neto, N.C., Pomeroy, A., Lowe, R., Ghisalberti, M., 2022. Seagrass meadows reduce wind-wave driven sediment resuspension in a sheltered environment. Front. Mar. Sci. 8, http://dx.doi.org/10.3389/fmars.2021.733542.

O'Driscoll, N.J., Covelli, S., Petranich, E., Floreani, F., Klapstein, S., Acquavita, A., 2019. Dissolved gaseous mercury production at a marine aquaculture site in the mercury-contaminated Marano and Grado Lagoon, Italy. Bull. Environ. Contam. Toxicol. 103, 218–224. http://dx.doi.org/10.1007/s00128-019-02621-1.

Philibert, A., Fillion, M., Silva, J.D., Lena, T.S., Mergler, D., 2022. Past mercury exposure and current symptoms of nervous system dysfunction in adults of a first nation community (Canada). Environ. Health: Glob. Access Sci. Source 21, http://dx.doi.org/10.1186/s12940-022-00838-y.

Picone, M., Distefano, G.G., Benhene, G.A., Corami, F., Basso, M., Panzarin, L., Carabelli, C., Ghirardini, A.V., 2023. Seabirds as biomonitors of mercury bioavailability in the Venice Lagoon. Bull. Environ. Contam. Toxicol. 110, http://dx.doi.org/10.1007/s00128-022-03650-z.

Poulain, A.J., Garcia, E., Amyot, M., Campbell, P.G., Raofie, F., Ariya, P.A., 2007. Biological and chemical redox transformations of mercury in fresh and salt waters of the high arctic during spring and summer. Environ. Sci. Technol. 41 (6), 1883–1888. http://dx.doi.org/10.1021/es061980b.

Rapaglia, J., Zaggia, L., Parnell, K., Lorenzetti, G., Vafeidis, A.T., 2015. Ship-wake induced sediment remobilization: Effects and proposed management strategies for the Venice Lagoon. Ocean Coast. Manag. 110, 1–11. http://dx.doi.org/10.1016/j.ocecoaman.2015.03.002.

Rasmussen, L.D., Turner, R.R., 1997. Cell-density-dependent sensitivity of a mer-lux bioassay. Appl. Environ. Microbiol. 63, 3291–3293.

Rosati, G., Canu, D., Lazzari, P., Solidoro, C., 2022. Assessing the spatial and temporal variability of MeHg biogeochemistry and bioaccumulation in the Mediterranean sea with a coupled 3D model. Biogeosciences 19, 3663–3682. http://dx.doi.org/10.5194/bg-2022-14.

Rosati, G., Heimbürger, L.E., Melaku Canu, D., Lagane, C., Laffont, L., Rijkenberg, M.J.A., Gerringa, L.J.A., Solidoro, C., Gencarelli, C.N., Hedgecock, I.M., De Baar, H.J.W., Sonke, J.E., 2018. Mercury in the black sea: new insights from measurements and numerical modeling. Glob. Biogeochem. Cycles 32 (4), 1–22. http://dx.doi.org/10.1002/2017GB005700.

Rosati, G., Solidoro, C., Canu, D., 2020. Mercury dynamics in a changing coastal area over industrial and postindustrial phases: Lessons from the Venice Lagoon. Sci. Total Environ. 743 (July), 1–15. http://dx.doi.org/10.1016/j.scitotenv.2020.140586.

Rossini, P., Guerzoni, S., Molinaroli, E., Rampazzo, G., Lazzari, A.D., Zancanaro, A., 2005. Atmospheric bulk deposition to the Lagoon of Venice: Part I. Fluxes of metals, nutrients and organic contaminants. Environ. Int. 31, 959–974. http://dx.doi.org/10.1016/j.envint.2005.05.006.

Sanz-Sáez, I., Pereira-García, C., Bravo, A.G., Trujillo, L., Ferriol, M.P.I., Capilla, M., Sánchez, P., Martín-Doimeadios, R.C.R., Acinas, S.G., Sánchez, O., 2022. Prevalence of heterotrophic methylmercury detoxifying bacteria across oceanic regions. Environ. Sci. Technol. 56, 3452–3461. http://dx.doi.org/10.1021/acs.est.1c05635.

Sarretta, A., Pillon, S., Molinaroli, E., Guerzoni, S., Fontolan, G., 2010. Sediment budget in the Lagoon of Venice, Italy. Cont. Shelf Res. 30 (8), 934–949. http://dx.doi.org/10.1016/j.csr.2009.07.002.

Schaefer, J.K., Yagi, J., Reinfelder, J.R., Cardona, T., Ellickson, K.M., Tel-Or, S., Barkay, T., 2004. Role of the bacterial organomercury lyase (MerB) in controlling methylmercury accumulation in mercury-contaminated natural waters. Environ. Sci. Technol. 38, 4304–4311. http://dx.doi.org/10.1021/es049895w.

Schartup, A.T., Mason, R.P., Balcom, P.H., Hollweg, T.a., Chen, C.Y., 2013. Methylmercury production in estuarine sediments: Role of organic matter. Environ. Sci. Technol. 47, 695–700. http://dx.doi.org/10.1021/es302566w.

Schartup, A.T., Ndu, U., Balcom, P.H., Mason, R.P., Sunderland, E.M., 2015. Contrasting effects of marine and terrestrially derived dissolved organic matter on mercury speciation and bioavailability in seawater. Environ. Sci. Technol. 49, 5965–5972. http://dx.doi.org/10.1021/es506274x.

Seelen, E.A., Chen, C.Y., Balcom, P.H., Buckman, K.L., Taylor, V.F., Mason, R.P., 2021. Historic contamination alters mercury sources and cycling in temperate estuaries relative to uncontaminated sites. Water Res. 190, 116684. http://dx.doi.org/10.1016/j.watres.2020.116684.

Seelen, E., Liem-Nguyen, V., Wünsch, U., Baumann, Z., Mason, R., Skyllberg, U., Björn, E., 2023. Dissolved organic matter thiol concentrations determine methylmercury bioavailability across the terrestrial-marine aquatic continuum. Nature Commun. 14, 6728. http://dx.doi.org/10.1038/s41467-023-42463-4.

Seelen, E.A., Massey, G.M., Mason, R.P., 2018. The role of sediment resuspension on estuarine suspended particulate mercury dynamics. Environ. Sci. Technol. 52 (14), 7736–7744. http://dx.doi.org/10.1021/acs.est.8b01920.

Sfriso, A., Birkemeyer, T., Ghetti, P.F., 2001. Benthic macrofauna changes in areas of Venice Lagoon populated by seagrasses or seaweeds. Mar. Environ. Res. 5 52, 323–349.

Sfriso, A., Marcomini, A., 1996. Decline of ulva growth in the Lagoon of Venice.

Sfriso, A., Mistri, M., Munari, C., Buosi, A., Sfriso, A.A., 2020. Management and exploitation of macroalgal biomass as a tool for the recovery of transitional water systems. Front. Ecol. Evol. 8, http://dx.doi.org/10.3389/fevo.2020.00020.

Sharif, A., Monperrus, M., Tessier, E., Bouchet, S., Pinaly, H., Rodriguez-Gonzalez, P., Maron, P., Amouroux, D., 2014. Fate of mercury species in the coastal plume of the Adour River estuary (Bay of Biscay, SW France). Sci. Total Environ. 496, 701–713. http://dx.doi.org/10.1016/j.scitotenv.2014.06.116.

Smagorinsky, J., 1963. General circulation experiments with the primitive equation I the basic experiment. Mon. Weather Rev. 91, 99–164.

Soerensen, A.L., Schartup, A.T., Gustafsson, E., Gustafsson, B.G., Undeman, E., Björn, E., 2016. Eutrophication increases phytoplankton methylmercury concentrations in a coastal sea—A baltic sea case study. Environ. Sci. Technol. 50 (21), 11787–11796. http://dx.doi.org/10.1021/acs.est.6b02717.

Soerensen, A.L., Sunderland, E.M., Holmes, C.D., Jacob, D.J., Yantosca, R.M., Skov, H., Christensen, J.H., a. Strode, S., Mason, R.P., 2010. An improved global model for air-sea exchange of mercury: High concentrations over the north atlantic. Environ. Sci. Technol. 44, 8574–8580. http://dx.doi.org/10.1021/es102032g.

Soetan, O., Nie, J., Feng, H., 2022. Preliminary environmental assessment of metal-contaminated sediment dredging in an Urban River, New Jersey, USA. Mar. Pollut. Bull. 184, http://dx.doi.org/10.1016/j.marpolbul.2022.114212.

Solidoro, C., Bandelj, V., Bernardi, F.A., Camatti, E., Ciavatta, S., Cossarini, G., Facca, C., Franzoi, P., Libralato, S., Canu, D.M., Pastres, R., Pranovi, F., Raicevich, S., Socal, G., Sfriso, A., Sigovini, M., Tagliapietra, D., Torricelli, P., 2010. Response of the Venice Lagoon ecosystem to natural and anthropogenic pressures over the last 50 years. In: Coastal Lagoons: Critical Habitats of Environmental Change. CRC press, Taylor & Francis Group, pp. 483–511. http://dx.doi.org/10.1201/EBK1420088304-c19, May 2014.

Solidoro, C., Pastres, R., Cossarini, G., Ciavatta, S., 2004. Seasonal and spatial variability of water quality parameters in the Lagoon of Venice. J. Mar. Syst. 51, 7–18. http://dx.doi.org/10.1016/j.jmarsys.2004.05.024.

Sprovieri, M., Oliveri, E., Di Leonardo, R., Romano, E., Ausili, A., Gabellini, M., Barra, M., Tranchida, G., Bellanca, A., Neri, R., Budillon, F., Saggiomo, R., Mazzola, S., Saggiomo, V., 2011. The key role played by the augusta basin (southern Italy) in the mercury contamination of the mediterranean sea. J. Environ. Monit. 13 (6), 1753. http://dx.doi.org/10.1039/c0em00793e.

Stoichev, T., Chanvalon, A.T.D., Veloso, S., Deborde, J., Tessier, E., Lanceleur, L., Amouroux, D., Chanvalon, A.T.D., 2022. Assessing and predicting the changes for inorganic mercury and methylmercury concentrations in surface waters of a tidal estuary (Adour Estuary, SW France). http://dx.doi.org/10.1016/j.marpolbul.2022.114400.

Stolpovsky, K., Dale, A.W., Wallmann, K., 2018. A new look at the multi-g model for organic carbon degradation in surface marine sediments for coupled benthic-pelagic simulations of the global ocean. Biogeosciences 15 (11), 3391–3407. http://dx.doi.org/10.5194/bg-15-3391-2018.

Sunderland, E.M., Gobas, F.A.P.C., Branfireun, B.A., Heyes, A., 2006. Environmental controls on the speciation and distribution of mercury in coastal sediments. Mar. Chem. 102 (1–2), 111–123. http://dx.doi.org/10.1016/j.marchem.2005.09.019.

Thomann, R., Di Toro, D., 1983. Physico-chemical model of toxic substances in the great lakes. J. Gt. Lakes Res. 9 (4), 474–496.

Umgiesser, G., Canu, D.M., Cucco, A., Solidoro, C., 2004. A finite element model for the Venice Lagoon. Development, set up, calibration and validation. J. Mar. Syst. 51 (1-4 SPEC. ISS.), 123–145. http://dx.doi.org/10.1016/j.jmarsys.2004.05.009.

Umgiesser, G., Canu, D.M., Solidoro, C., Ambrose, R., 2003. A finite element ecological model: a first application to the Venice Lagoon. Environ. Model. Softw. 18, 131–145. http://dx.doi.org/10.1016/S1364-8152(02)00056-7.

Umgiesser, G., Ferrarin, C., Cucco, A., Pascalis, F.D., Bellafiore, D., Ghezzo, M., Bajo, M., 2014. Comparative hydrodynamics of 10 mediterranean lagoons by means of numerical modeling. J. Geophys. Res.: Oceans 119, 2212–2226. http://dx.doi.org/10.1002/2013JC009512.

Winter, C., 2007. On the evaluation of sediment transport models in tidal environments. Sediment. Geol. 202, 562–571. http://dx.doi.org/10.1016/j.sedgeo.2007.03.019.

Wool, T., Ambrose, R., Martin, J., Comer, E., 2001. Water quality analysis simulation program (WASP) version 6.0: User's manual.

Zhang, Y., Jacob, D.J., Dutkiewicz, S., Amos, H.M., Long, M.S., Sunderland, E.M., 2015. Biogeochemical drivers of the fate of riverine mercury discharged to the global and Arctic oceans. Glob. Biogeochem. Cycles 29, 854–864. http://dx.doi.org/10.1002/2015GB005124.

Zhang, Y., Jacob, D.J., Horowitz, H.M., Chen, L., Amos, H.M., Krabbenhoft, D.P., Slemr, F., Louis, V.L.S., Sunderland, E.M., 2016. Observed decrease in atmospheric mercury explained by global decline in anthropogenic emissions. Proc. Natl. Acad. Sci. 113, 526–531. http://dx.doi.org/10.1073/pnas.1516312113.

Zhang, H., Moffett, K.B., Windham-Myers, L., Gorelick, S.M., 2014. Hydrological controls on methylmercury distribution and flux in a tidal marsh. Environ. Sci. Technol. 48, 6795–6804. http://dx.doi.org/10.1021/es500781g.

Zhang, Y., Soerensen, A.L., Schartup, A.T., Sunderland, E.M., 2020. A global model for methylmercury formation and uptake at the base of marine food webs. Glob. Biogeochem. Cycles 34, 1–21. http://dx.doi.org/10.1029/2019GB006348.

Zonta, R., Botter, M., Cassin, D., Bellucci, L.G., Pini, R., Dominik, J., 2018. Sediment texture and metal contamination in the Venice Lagoon (Italy): A snapshot before the installation of the MOSE system. Estuar. Coast. Shelf Sci. 205, 131–151. http://dx.doi.org/10.1016/j.ecss.2018.03.007.